The Journal of Experimental Biology 210, 4319-4334
Published by The Company of Biologists 2007
doi:10.1242/jeb.010389

Turning behaviour depends on frictional damping in the fruit fly *Drosophila*

Thomas Hesselberg and Fritz-Olaf Lehmann*

Biofuture Research Group, Institute of Neurobiology, University of Ulm, Albert-Einstein-Allee 11, 89081 Ulm, Germany

*Author for correspondence (e-mail: fritz.lehmann@uni-ulm.de)

Accepted 16 October 2007

Summary

Turning behaviour in the fruit fly *Drosophila* depends on several factors including not only feedback from sensory organs and muscular control of wing motion, but also the mass moments of inertia and the frictional damping coefficient of the rotating body. In the present study we evaluate the significance of body friction for yaw turning and thus the limits of visually mediated flight control in *Drosophila*, by scoring tethered flies flying in a flight simulator on their ability to visually compensate a bias on a moving object and a visual background panorama at different simulated frictional dampings. We estimated the fly's natural damping coefficient from a numerical aerodynamic model based on both friction on the body and the flapping wings during saccadic turning. The model predicts a coefficient of 54×10^{-12} Nm s, which is more than 100-times larger than the value estimated from a previous study on the body alone. Our estimate suggests that friction plays a larger role for yaw turning in *Drosophila* than moments of inertia. The simulator experiments showed that visual performance of the fruit fly collapses near the physical conditions estimated for freely flying animals, which is consistent with the suggested role of the halteres for flight stabilization. However, kinematic analyses indicate that the measured loss of flight control might be due predominantly to the limited fine control in the fly's steering muscles below a threshold of 1–2° stroke amplitude, rather than resulting from the limits of visual motion detection by the fly's compound eyes. We discuss the impact of these results and suggest that the elevated frictional coefficient permits freely flying fruit flies to passively terminate rotational body movements without producing counter-torque during the second half of the saccadic turning manoeuvre.

Key words: flight control, flight saccade, visual system, body friction, steering capacity.

Introduction

Our understanding of the aerodynamic mechanisms behind lift and thrust production in flying insects has improved tremendously during the past decade. The discovery of unsteady and three-dimensional aerodynamic effects such as rotational circulation, wake capture and attached leading edge vortices, offers a satisfactory explanation of how many insects remain airborne and produce flight forces of up to twice their body weight (e.g. Dickinson et al., 1999; Ellington et al., 1996; Marden, 1987; Willmott et al., 1997). Force control generally differs among species (Taylor, 2001) and flying insects control forces and moments using a large variety of different kinematic manoeuvres such as changes in wing stroke amplitude and frequency (e.g. Kutsch and Gewecke, 1979; Lehmann and Dickinson, 1997; Lehmann and Dickinson, 1998), the wing's angle of attack (e.g. Dudley and Ellington, 1990; Alexander, 1986; Zarnack, 1988), speed and timing of wing rotation (Alexander, 1986; Dickinson et al., 1993), kinematic phase between ipsilateral fore- and hindwing motion in four-winged insects (Alexander, 1986; Berger and Kutsch, 2003), alterations in body angle with respect to the horizontal (David, 1978; Dudley and Ellington, 1990; Wakeling and Ellington, 1997), and deflections of the abdomen and legs (Zanker, 1988).

Besides the control for adjusting translational forces such as thrust and body lift, yaw turning during manoeuvring flight has attracted considerable interest, because it determines flight heading and is thus of augmented ecological relevance for foraging behaviour and search strategies in insects. Yaw turning behaviour in an insect depends on multiple factors such as (i) the time course of yaw torque production and thus the temporal changes in motion of wings and other body appendages, (ii) the constraints on sensory feedback mainly coming from the compound eyes and, in flies, from gyroscopic halteres, and (iii) on the physics of turning such as the moments of body inertia and frictional damping between the various body structures and the surrounding air.

Results from both tethered (Götz, 1968; Götz, 1983) and free-flight (Fry et al., 2003) experiments showed that the fruit fly *Drosophila* generates yaw torque mainly by producing differences in wing stroke amplitude and stroke plane between the two beating wings. The latter authors suggest that changes in angle of attack and consequently the timing of wing rotation at the stroke reversal only play a minor role for yaw control, although a robotic *Drosophila* model wing showed that even moderate changes in rotational timing may tremendously alter lift and drag production of a flapping wing (Dickinson et al.,

1999). Wing stroke frequency can be ruled out as a parameter for flight control during yaw turning since the mechanical linkage prevents the wings from operating at asymmetric frequencies (Hollick, 1940). Abdominal deflections to the side of the turn have also been associated with torque production in tethered fruit flies (Zanker, 1988); however, with a response time of seconds, abdominal steering is unlikely to be of great significance during a saccadic flight style during which the fly turns approximately 90° in 50–100 ms (Fry et al., 2003; Tammero and Dickinson, 2002b).

The physical parameters predominantly determining yaw turning rate are the frictional damping coefficient and the mass moments of inertia of the fly. The former is a measure of the importance of air friction, where higher frictional damping results in a lower peak angular velocity at constant yaw torque production. By contrast, mass moment of inertia determines how quickly the animal may alter its angular velocity around the vertical body axis. Elevated frictional damping and moments of inertia favour stable flight because these factors reduce both angular acceleration and maximum angular velocity while they impair manoeuvrability (Fry et al., 2003; Hedrick, 2007; Hedrick et al., 2007; Mayer, 1988). The conventional view on friction and inertia in flies is that flight is friction-dominated (Reichardt and Poggio, 1976), yet a recent study by Fry et al. (Fry et al., 2003) on saccadic turning in freely flying *Drosophila* refuted this assumption, suggesting that turning motion is dominated by the fly's mass moments of inertia. Despite the elegance of the latter study, this conclusion is based on frictional damping estimated by an integration of Stokes' law for the fly body only and ignores changes in drag on the flapping wings during turning. Since even small changes in wing velocity due to body rotation result in significant changes in drag production, the authors may thus have underestimated frictional damping.

Moreover, the low frictional damping coefficient in *Drosophila* was recently questioned by studies on the time course of torque production during flight saccades using three-dimensional unsteady computations (Ramamurti and Sandberg, 2007) and kinematic measurements in magnetically tethered fruit flies (Bender and Dickinson, 2006a). The latter study highlights the inconsistency between the torque estimated at low friction and the earlier calculations, because the derived peak torque below 0.2×10^{-9} Nm during turning would require a frictional coefficient that is 350 times larger than the previous estimate. Although Bender and Dickinson favoured an alternative explanation based on the pitch-enhancing clap-and-fling mechanism, the discrepancy between the two estimates for damping coefficient in *Drosophila* persists. Since a significantly larger frictional coefficient works against angular motion and might thus, for example, even reduce the need of active braking during the second half of a flight saccade, a behavioural estimation of the significance of damping coefficient based on both body and wing motion is desirable. Wing-based damping in wing amplitude asymmetry-driven turning has previously been reported for freely flying cockatiels and cockatoos and recognized as an important mechanism for roll dynamics during aerodynamic reorientation (Hedrick, 2007; Hedrick et al., 2007). The latter studies, for example, have shown that the roll damping coefficient in birds is 2–6 times greater than the coefficients typical of airplane flight dynamics, which greatly limits roll magnitude during manoeuvring flight in these animals.

In this study we therefore investigate how turning performance in the fruit fly *Drosophila* changes with changing friction on body and wings. To achieve this goal, we developed a numerical model based on drag that acts on the flapping insect wings, using a quasi-steady aerodynamic approach. Moreover, to evaluate the significance of visual motion detection for object orientation behaviour and flight stabilization at various damping coefficients, we present a numerical model that predicts the required precision for kinematic control during manoeuvring flight. Tethered animals were flown in a closed-loop flight simulator and scored on their ability to compensate a velocity bias on a single black object and a random-dot visual panorama, over a large range of different simulated frictional damping coefficients for yaw turning. From the above approaches and experiments we eventually conclude that friction plays a key role for yaw turning behaviour in *Drosophila* because it determines both the precision with which the animal needs to control the torque around its vertical axis and potentially also the need for gyroscopic organs such as halteres for sensory feedback.

Materials and methods

Animals

All experiments were carried out on 2–5-day-old female Canton S wild-type *Drosophila melanogaster*. The flies were selected from a laboratory colony maintained at 24°C on commercial *Drosophila* food (Carolina Biological, Burlington, NY, USA). We anaesthetised the animals by cooling them to approximately 4°C on a Peltier stage. The flies were then tethered between the head and the notum to a 7.3 mm long, 0.13 mm diameter tungsten rod using UV-light activated glue (Clear Glass Adhesive, Henkel Loctite, Düsseldorf, Germany). Curing time was 20 s using a 150 W Osram halogen lamp. Each fly was given a small moist tissue on which to rest and allowed at least 1 h to recover before we placed them in the flight simulator.

Flight simulator

The flight simulator used in this study has already been described in detail (Lehmann and Dickinson, 1997), so only a brief introduction is given here. The tungsten rod on the tethered flies fit into a holder that placed the fly in the middle of a cylindrical flight simulator, 125 mm high and 150 mm in diameter (Fig. 1A). The holder ensured that the fly was in a hovering position, with a body angle of 60°, so that the stroke plane of the wings coincided with the horizontal (David, 1978). An infra-red diode above the flight simulator cast shadows of the wings on an infra-red sensitive mask connected to a wing stroke analyser that provided wing stroke amplitudes and frequencies for each single stroke cycle. We calibrated wing stroke amplitudes by digitizing the wing positions on video images of the flying animal recorded by an infra-red sensitive camera. The voltages coming from the infra-red light path were subsequently converted into degrees employing linear regression on the digitised data. Both digitization and the final calibration were done with custom-built Origin (Version 7, OriginLab Corporation, MA, USA) routines.

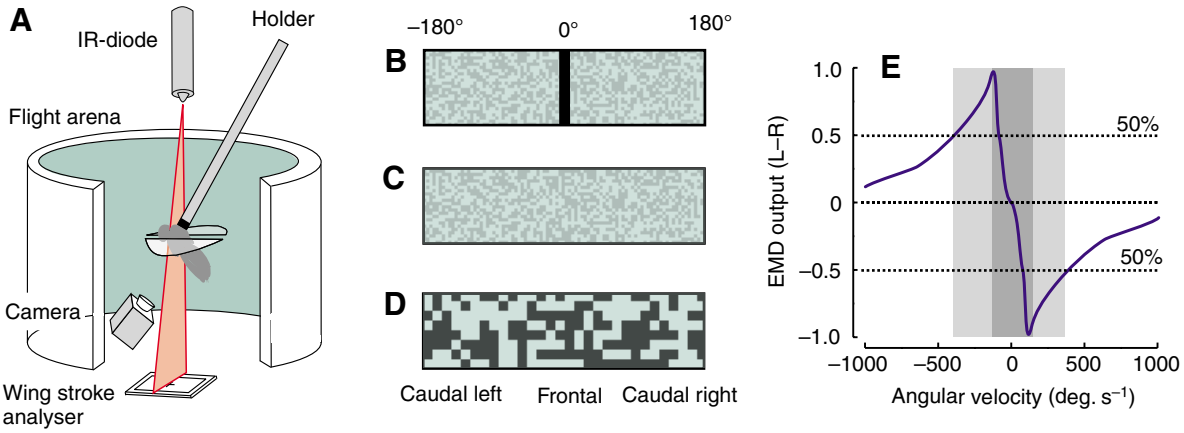

Fig. 1. Closed-loop feedback flight simulator. (A) The animals were placed in the centre of the simulator and modulated their wing stroke amplitudes in response to visual stimuli. An infra-red light cast shadows of the wings on a wing stroke analyser and an infra-red camera tracked the wings for calibration. Schematics not to scale. (B–D) Patterns displayed inside the simulator. (E) Output of a 1-D, 72-receptor-wide model of the fly's elementary motion detector (EMD) to rotation of a 24° spatial wavelength stripe pattern (M. Mronz and F.-O. Lehmann, manuscript submitted for publication). Dark grey areas indicate 100 (±125 deg. s^{-1}) and light grey areas 50% (±390 deg. s^{-1}) response threshold. L, left eye; R, right eye.

The 360° simulator consisted of 180 green-light-emitting diodes in the horizontal and 48 in the vertical plane. A conventional computer generated two types of visual environments: a 12° wide black bar foreground pattern and a random-dot background. A more detailed description of the patterns is given below. The fly actively controlled the azimuth velocity of the two patterns by changing the relative difference of the stroke amplitude between left and right flapping wing (left-minus-right). The image displayed in the simulator was updated every 8 ms and flickered with a frequency of 1000 Hz, which is well above *Drosophila*'s flicker fusion rate of around 200 Hz (Autrum, 1958).

Physics engine

To simulate visual feedback conditions for various damping coefficients, we developed a physics engine that derives the angular velocity of a visual panorama from the animal's torque production, T, its mass moments of inertia I and the frictional damping coefficient C. According to Fry et al. (Fry et al., 2003), instantaneous yaw torque of the animal may be written as:

$$T(t) = I\dot{\omega}(t) + C\omega(t) \,, \tag{1}$$

where t is time, the parameter $\dot{\omega}(t)$ is the instantaneous angular acceleration, and $\omega(t)$ is instantaneous angular velocity or simulated turning velocity of the fly. The latter equation assumes rotation constrained about the yaw axis and does not predict yaw torque correctly during a free flight saccade mixed with roll and pitch. We converted our measurements of wing stroke amplitude into yaw torque using the relationship between wing motion and torque measured in tethered fruit flies under optomotor stimulation (Götz, 1983). From these data we deduced the following linear relationship between torque and difference in stroke amplitude:

$$T(t) = k\Delta\Phi_{\mathrm{L-R}}(t) \,, \tag{2}$$

in which the constant k is 2.9×10^{-10} Nm deg^{-1} stroke amplitude and $\Delta\Phi_{\mathrm{L-R}}(t)$ is the instantaneous difference in stroke amplitude between the left and the right wing. Instantaneous angular acceleration of the panorama $\dot{\omega}(t)$ is equal to the difference in angular velocity between two time steps dt (8 ms) and may be expressed by:

$$\dot{\omega}(t) = \frac{\omega(t) - \omega(t-1)}{\mathrm{d}t} \,. \tag{3}$$

Eventually, by combining the above equations, we may iteratively determine the angular velocity of the visual panorama from the following equation:

$$\omega(t) = \frac{k\Delta\Phi_{\mathrm{L-R}}(t) + \left(\frac{I}{\mathrm{d}t}\right)\omega(t-1)}{C + \left(\frac{I}{\mathrm{d}t}\right)} \,. \tag{4}$$

Eqn 4 is the core of the physics engine and was implemented in the software that controlled the pattern of the flight simulator (C++ 6.0, Microsoft Corporation, Redmond, WA, USA). During the experiments the moment of inertia and the damping coefficient could be set from a software control panel that allowed us easily to change the physical conditions of feedback simulation.

Modelling minimum torque from visual threshold

To estimate the limits of visually mediated yaw torque control in our simulator, we determined the torque required for controlling the visual pattern. The model is based on the assumption that the angular velocity of the visual panorama during manoeuvring flight should not exceed the threshold for visual motion detection of the animal. We determined the visual threshold from a previously constructed model of the output of a one-dimensional (1-D) 'Hassenstein-Reichardt' elementary motion detector (EMD) array. This array consisted of 72, equally spaced 5° wide ommatidia and modelled the fly's

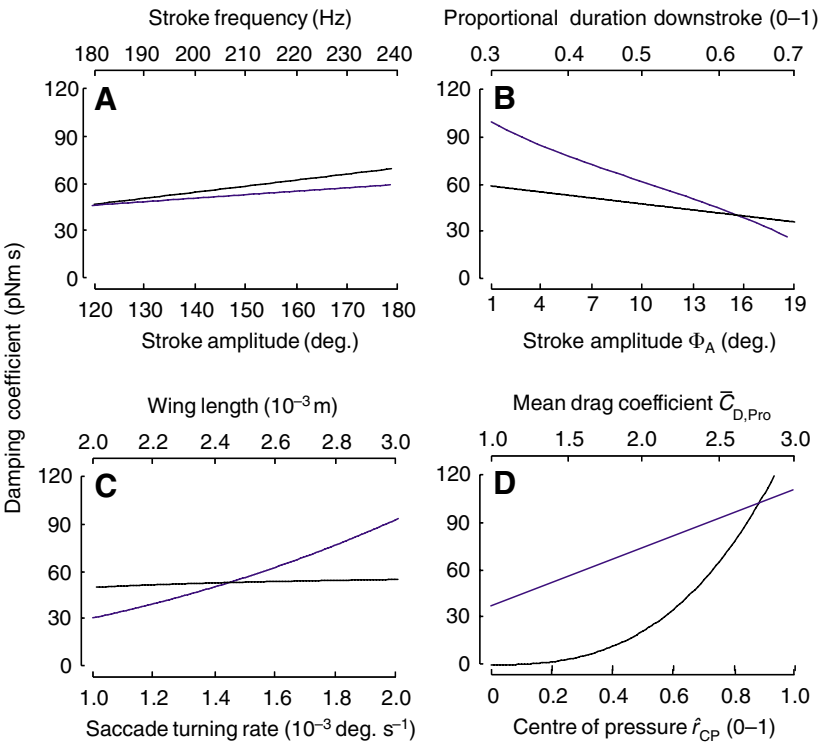

Fig. 2. Alterations in the prediction of the numerical damping model to changes in morphometrics and kinematic parameters. Damping coefficient plotted as a function of (A) stroke amplitude (black line) and frequency (blue line), (B) active amplitude component Φ_A (black line) and relative duration of the downstroke (blue line), (C) turning rate within a flight saccade (black line) and wing length (blue line), and (D) centre of pressure (black line) and mean drag coefficient (blue line).

horizontal eye region (M. Mronz and F.-O. Lehmann, manuscript submitted for publication) (Kern and Egelhaaf, 2000). By simulating the response to angular motion of a stripe pattern with 24° spatial wavelength (12° black stripes), we found that maximum and 50% response of the EMD system occurred at an angular rotation of 125 and 390 deg. s^{-1}, respectively (Fig. 1E). Assuming that these values characterize the upper threshold range at which the visual system of *Drosophila* is able to detect visual motion, we may modify Eqn 1 and Eqn 2 towards a time-invariant version that yields:

$$\Delta\Phi_{L-R,Max} = \frac{I\left(\frac{\omega_V}{t_V}\right) + C\omega_V}{k}, \quad (5)$$

in which ω_V is the limit of angular retinal speed allowing the fly to visually determine its angular rotation, and the ratio ω_V/t_V is the maximum angular acceleration between the upper limit of the angular retinal speed and the visuo-motor reaction time t_V of the fly. The latter value amounts to 30 ms and was estimated from a previous behavioural study on male–female chases in houseflies *Musca* (Land and Collett, 1974). Most of this delay appears to be due to the time-to-peak response of the photo-transduction process, i.e. 12 and 41 ms for the dark- and light-adapted state of the housefly's compound eye, respectively (Howard et al., 1984). The values reported for *Drosophila* are similar to those of *Musca* and range from 20 to 50 ms bump latency (Hardie and Raghu, 2001). Thus, we do not expect that *Drosophila* exhibits a significantly faster reaction time during free flight due to its smaller body size.

Frictional damping

Throughout the experiments described in this study, we kept yaw moment of inertia for *Drosophila* constant at a value of 0.52×10^{-12} Nm s^2. This estimate results from the fly's body morphology and was derived from a standard formula for a cylinder, rotating around its central traverse axis (Fry et al., 2003). The latter study also estimated a frictional damping coefficient for the fly body during natural conditions of approximately 0.52×10^{-12} Nm s using an integration of Stokes' law. However, since this method ignored frictional damping on the flapping wings, we here present an alternative approach.

The model represents a time-invariant approach, assuming mean values for wing velocity and body rotation during saccadic turning. In particular, we assume that angular velocity of body rotation is constant for the most part of the saccade, as found by Fry et al. (Fry et al., 2003), although other free flight studies suggest a constantly increasing and decreasing angular velocity profile during turning (M. Mronz and F.-O. Lehmann, manuscript submitted for publication) (Tammero and Dickinson, 2002b). The latter studies, however, did not report the difference in wing stroke amplitudes needed for our simulation. The model followed a five-step procedure: (i) we first estimated mean wing velocity for both wings during straight flight assuming a sinusoidal velocity profile during up- and downstroke. (ii) To these estimates we added the active changes in wing stroke amplitude during saccadic turning and (iii) also the angular components resulting from the flies' body rotation. (iv) Subsequently, we calculated the velocity differential between both wings and (v) calculated drag based on yaw damping from the velocity differentials, assuming horizontal wing motion during hovering. In the theoretical framework, we considered the fly's wing kinematics during a saccadic turn clockwise. The model is explained in greater detail in the Appendix.

To test the robustness of our damping estimate, we plotted the changes in coefficient as a function of stroke amplitude and frequency (Fig. 2A), active amplitude component Φ_A and up- to downstroke ratio (Fig. 2B), rotational velocity of the body within saccade and wing length (Fig. 2C), and centre of pressure and mean drag coefficient (Fig. 2D). The data obtained from the plotted parameter range suggest that our damping coefficient is most sensitive to the ratio between up- and downstroke, wing length and centre of pressure; however, it did not drop below approximately 20×10^{-12} Nm s for the range of estimates published for *Drosophila* wing motion. In the experiments presented in this paper, we tested the behavioural response of

Table 1. *Morphometrics, aerodynamic and kinematic parameters of Drosophila melanogaster used for numerical modelling during saccadic clockwise turning*

Symbol	Description	Value	Reference
Φ_F	Wing stroke amplitude	140° (2.44 rad)	(Fry et al., 2005)
n	Wing stroke frequency	218 Hz	(Fry et al., 2005)
$\bar{\omega}$	Saccadic turning rate	1600 deg. s^{-1} (27.9 rad s^{-1})	(Fry et al., 2003)
$\hat{t}$	Relative duration of downstroke	0.538	(Fry et al., 2005)
$\Phi_{P,U}$	Passive wing stroke difference upstroke	4.0° (0.069 rad)	This study
$\Phi_{P,D}$	Passive wing stroke difference downstroke	3.4° (0.059 rad)	This study
Φ_A	Mean active wing stroke difference	5° (0.087 rad)	(Fry et al., 2003)
$\hat{r}_{CP}$	Distance to centre of pressure	0.7	(Ramamurti and Sandberg, 2001)
R	Wing length	2.51×10^{-3} m	This study
W	Thorax width	1.1×10^{-3} m	This study
ρ	Density of air	1.2 kg m^{-3}	(Vogel, 1994)
$\bar{C}_{D,Pro}$	Mean profile drag of wing	1.46	(Fry et al., 2005)
S	Surface area of one wing	2.0×10^{-6} m^2	(Lehmann and Dickinson, 1997)
$\lvert d\hat{\phi}/d\hat{t}\rvert$	Dimensionless wing velocity	4.4	(Fry et al., 2005)

the animals at the following frictional damping coefficients: 52, 156, 208, 260, 520, 1040, 2080 and 5200×10^{-12} Nm s, corresponding to a 100-fold range in time constants (I/C) from approximately 0.1 to 10 ms. Since pilot experiments showed that the flies could not control the visual panorama at a damping of 0.52×10^{-12} Nm s, we excluded this value from our analysis.

To numerically evaluate the potential effect of the various frictional coefficients on a rotating model fruit fly, we plotted the angular velocity changes over time at the various dampings and assumed a constant torque of 29×10^{-10} Nm deg.$^{-1}$ that equals approximately 10° relative wing stroke amplitude between both wings (Eqn 4, Table 1, Fig. 3B). The model predicts that the animal reaches peak angular velocity within approximately one wing stroke (5 ms) and six wing strokes (30 ms) at high ($520–5200\times10^{-12}$ Nm s) and low frictional coefficients ($0.52–260\times10^{-12}$ Nm s), respectively. The grey area in Fig. 3B shows the thresholds of the visual system for motion detection (cf. Fig. 1E).

Behavioural tests

To evaluate the behavioural effect of frictional damping on visually mediated flight performance in tethered fruit flies, we employed two experimental approaches: (i) a test of the animal's ability to visually stabilize a vertical black stripe in the frontal region of both compound eyes (object orientation or fixation behaviour) and (ii) a test in which we scored flies on their ability to stabilize a random-dot background pattern within the simulator with their optomotor reflexes (Heisenberg and Wolf, 1984). We scored a total of 47 females, all continuously exhibiting wing stroke amplitudes above 100° and wing beat frequencies above 180 Hz. Total flight time of each fly was 360 s divided into sequences of 45 s, in which we confronted the animal with the eight frictional dampings (see Fig. 3B) presented in random order.

In the first set of experiments, the visual panorama consisted of two visual patterns: a 12° (6×49 pixels) wide black stripe as a foreground pattern and a low-contrast 2×2 pixel white and

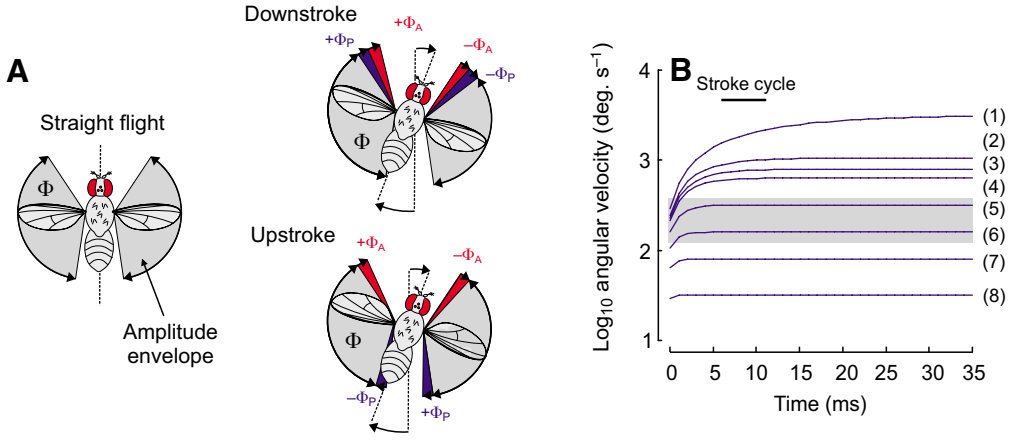

Fig. 3. Modelling damping coefficient in *Drosophila*. (A) During yaw turning, stroke amplitude changes due to an active component (Φ_A) caused by the fly's steering muscles, and passive changes (Φ_P) due to body rotation. Note the different contribution of passive components during the stroke cycle (downstroke, top; upstroke, bottom). (B) Turning rate of a fruit fly in response to the impulsive start of yaw torque. Data were modelled at different frictional damping coefficients, at a constant torque of 0.29 pNm, and 0.52 pNm s^2 moment of inertia. Numbers in parentheses (1–8) correspond to damping coefficients 52, 156, 208, 260, 520, 1040, 2080 and 5200 pNm s, respectively. The shaded area indicates the maximum threshold range for visual motion detection (cf. Fig. 1E).

grey (25% black) pixels random-dot pattern in the background (Fig. 1B). Both patterns were under closed-loop feedback, but the foreground stripe sinusoidally moved according to a small velocity bias that caused changes in angular positions of ±48° within a period of 2 s. We applied this bias in order to continuously face the flies with a steering task and because motion of the stripe relative to the background should increase fixation performance (Heisenberg and Wolf, 1984). In other words, the relative motion between fore- and background pattern emulated free flight conditions, in which the flies were constantly attempting to follow a visual object that moved independently in front of the background. Fixation and anti-fixation were defined to occur when the flies continuously maintained the stripe in a 90° frontal (±45°) and caudal region (±135–180°) of their visual field for at least 1 s, respectively (Fig. 1). We calculated the 'fixation index' from the total time the animal spent fixating the stripe divided by the total flight time in a sequence.

In the second set of experiments, we investigated to what degree fruit flies may visually stabilize the simulator panorama in closed-loop without interference of a foreground pattern (Heisenberg and Wolf, 1984). To allow a comparison between both sets of experiments, we tested the fly's response to two backgrounds: (i) a 'poor' visual environment, in which the animals were exposed to the same low-contrast, small dot background as in the object orientation experiments, but without the stripe (Fig. 1C), and (ii) a 'rich' visual environment in which the flies faced a high-contrast pattern (100% contrast) with a larger spatial wavelength (6×6 pixel dots, Fig. 1D). In both optomotor experiments, we applied the same sinusoidal velocity bias to the panorama that had been applied to the vertical stripe in the object orientation experiments.

Analysis

To quantify the precision with which the animals compensated for the velocity bias on the visual panorama, we modelled the requirements for flight control by deriving the relative stroke amplitude between both wings required to fully compensate for the bias. We started the simulation by deriving the relative position of the visual object (stripe), ψ, inside the flight simulator using the following equation:

$$\psi = A \sin\left(\frac{2\pi}{T} t\right), \tag{6}$$

where A is the amplitude in azimuth motion of the pattern (48°) and T is the cycling period (2 s). The velocity bias and thus angular velocity of the panorama, $\dot{\psi}$, is equal to the derivative of Eqn 6 that may be expressed as:

$$\dot{\psi} = A \frac{2\pi}{T} \cos\left(\frac{2\pi}{T} t\right). \tag{7}$$

According to Eqn 1, yaw torque depends on the product between the moment of inertia and angular acceleration of the fly and, in the simulator, on angular acceleration of the visual panorama, $\ddot{\psi}$. We derived this measure by differentiating Eqn 6 a second time, which yields:

$$\ddot{\psi} = -A \left(\frac{2\pi}{T}\right)^2 \sin\left(\frac{2\pi}{T} t\right). \tag{8}$$

In a final step, we combined Eqn 1 and Eqn 2 and replaced angular velocity and acceleration of the fly by those terms determined for the visual panorama (Eqn 7 and Eqn 8). The following equation thus allows us to determine the instantaneous difference in wing stroke amplitude between both wings that is required to fully stabilize the visual panorama during flight, i.e.:

$$\Delta\Phi_{\mathrm{L-R}} = \frac{\ddot{\psi} I + \dot{\psi} C}{k}. \tag{9}$$

The difference between the simulated kinematics and the fly's actual wing motion in an experiment was eventually used to score how the animal coped with the elicited visual perturbations at the various feedback conditions.

Statistics

If not stated otherwise, we performed statistical tests on mean values, employing two-way ANOVA for repeated measurements in which damping coefficient was treated as a within-subjects effect. Behavioural data measured in the same animal and in different (e.g. experiments using the two random-dot background patterns) animals were treated as within- and between-subjects effects, respectively. We applied the Greenhouse–Geisser correction in cases where the Mauchly's Test for Sphericity showed violations. However, in none of the statistical tests did the latter correction alter the outcome of the statistics. In cases where the between-subjects effects were significant, we employed a Tamhane T2 *post hoc* test, which does not assume equal variances. The significance level was set at 5% and all calculations were performed using SPSS (Version 10.0, SPSS Inc. 1999). We removed flies from the analyses that showed no fixation behaviour at any of the frictional damping coefficients and, for statistical comparison, also data measured at 52×10^{-12} Nm s damping, at which none of the animals were able to keep the visual object for at least 1 s in the frontal region of the compound eye. Throughout the text averaged values are given as means ± standard deviation (s.d.).

Results

Object orientation experiments

The vast majority of flies tested in the flight simulator tried to maintain the stripe in the frontal region of their compound eyes. However, the time traces in Figs 4–6 show that this behaviour depended on the frictional damping coefficient applied during visual feedback simulation. The three figures represent three aspects of flight behaviour: Fig. 4 shows the differences in stroke amplitude between both wings (blue) superimposed with the simulated response (Eqn 9) required to fully compensate for the velocity bias (red), while Fig. 5 shows the corresponding angular azimuth velocity of the stripe. The grey areas in Figs 4 and 5 represent the time at which fixation behaviour occurred. By contrast, Fig. 6 demonstrates the corresponding position of the black stripe (blue) during flight

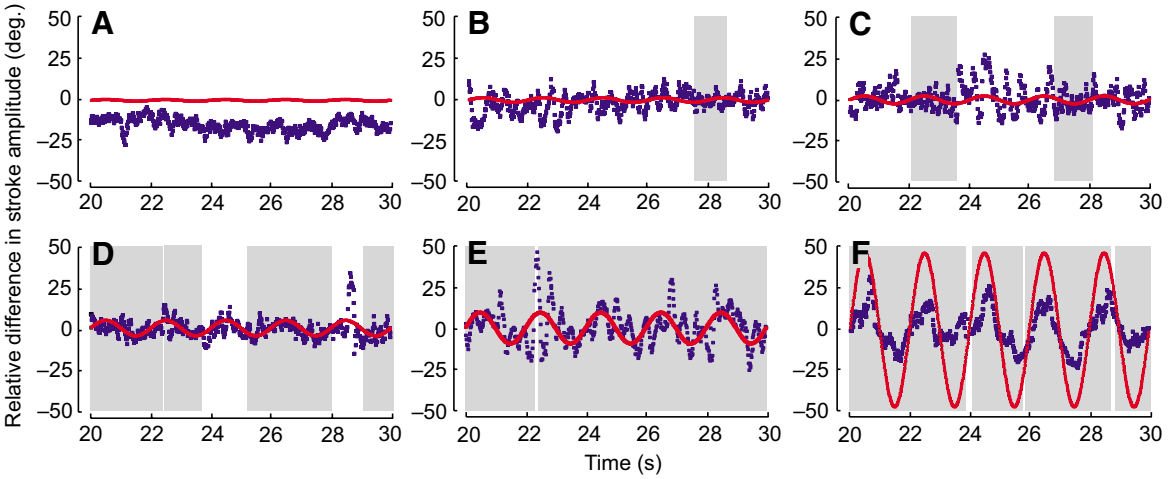

Fig. 4. Difference in stroke amplitude (left-minus-right wing, blue) of *Drosophila melanogaster* while responding to the black stripe. Time traces show the fly's behaviour 10 s after switching on the stimulus bias. (A–F) Flight at the damping coefficients 52, 156, 260, 520, 1040 and 5200 pNm s, respectively. The outcome of the numerical model for compensation of the velocity bias (Eqn 9) is shown in red. The visual target (black stripe) oscillated with an amplitude of ±48° and 0.5 Hz. The shaded areas indicate fixation behaviour. Positive (negative) differences indicate clockwise (counter clockwise) rotation.

where the frontal window used to quantify fixation behaviour is shown in grey.

At low damping coefficients between 52 and 260×10^{-12} Nm s, the animals were usually not able to compensate for the velocity bias and thus for the stripe movements, for any length of time (Fig. 4A–C). The flies either (i) completely lost control, (ii) failed to modulate the wing stroke difference around zero, which caused the stripe to rotate at a velocity above the threshold of their visual system like under an open-loop condition (Figs 4A–6A), or (iii) succeeded in modulating the velocity near the visual threshold but overshot the required differences in wing stroke amplitude. By contrast, at higher frictional damping coefficients between 520 and 5200×10^{-12} Nm s, most of the animals successfully matched their wing stroke amplitude difference with the requirements to compensate for the bias and thus continuously kept the angular velocity of the stripe below the threshold of the visual system, resulting in fixation behaviour (Figs 4–6E,F). The differences between the numerical model and the behavioural data are addressed later in the Results, when we compare the flies' behaviour during object orientation with their optomotor responses.

Fig. 7 summarizes the time traces of the tested flies, showing mean values of (i) the relative proportion of fixation and anti-fixation behaviour in the flight sequences (Fig. 7A), (ii) the azimuth velocity of the vertical stripe (Fig. 7B) and the position probability of the stripe inside the simulator as a histogram (Fig. 7C). The time during which the flies were able to stabilize the stripe in the frontal window significantly depends on damping coefficient (one-way ANOVA: $F_{6,138}$=47.1, P<0.001,

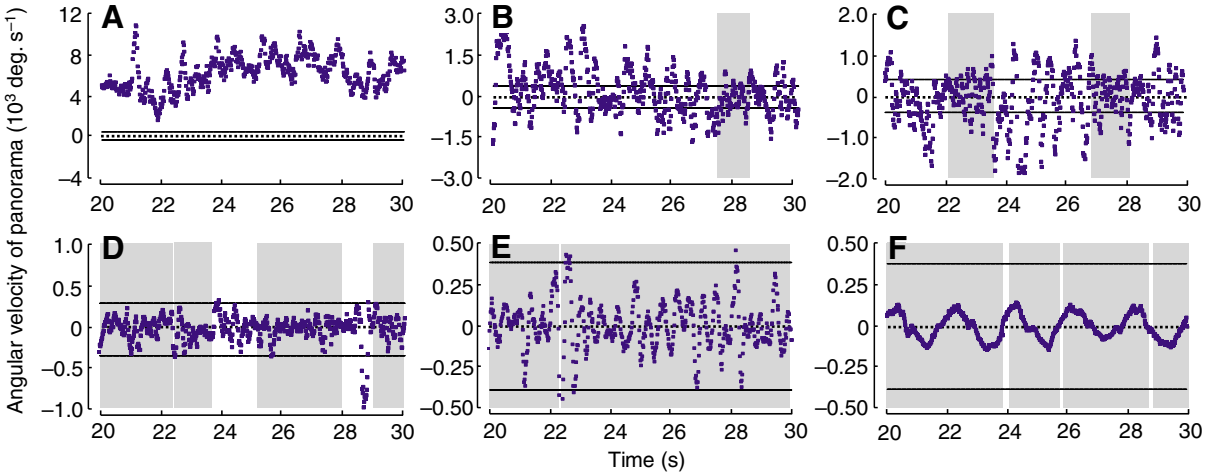

Fig. 5. Angular velocity of the visual panorama while the animal tried to keep the black stripe in the frontal position of the compound eyes. Data correspond to the time traces shown in Fig. 4. (A–F) Flight at the damping coefficients 52, 156, 260, 520, 1040 and 5200 pNm s, respectively. Solid black lines indicate the threshold (±390 deg. s^{-1}) for visual motion detection (50% response, Fig. 1E). See Fig. 4 for more details. Positive (negative) velocities indicate clockwise (counter clockwise) rotation.

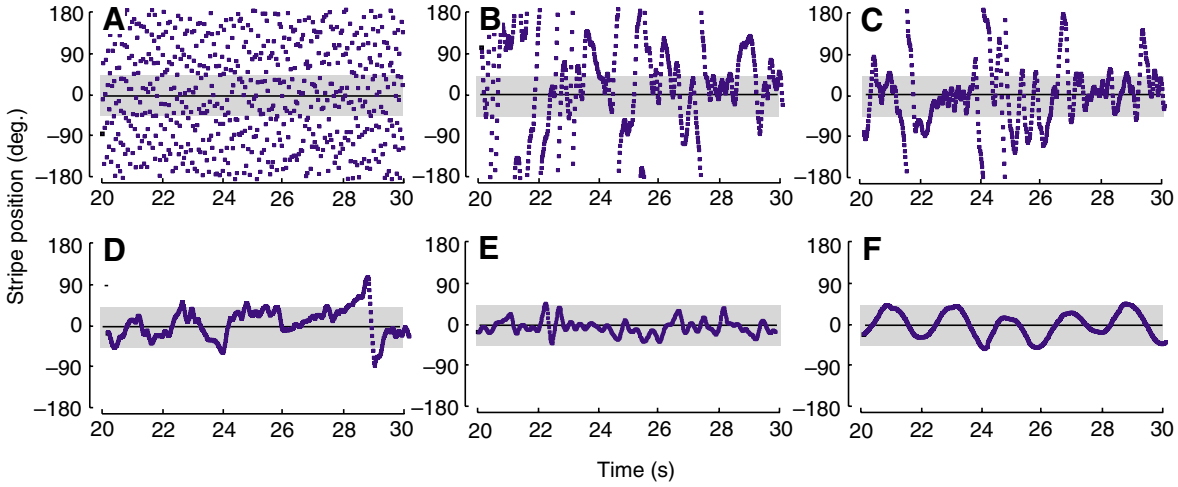

Fig. 6. Position of the black stripe inside the visual panorama during flight (Fig. 1B). Data correspond to the time traces shown in Figs 4 and 5. (A–F) Flight at the damping coefficients 52, 156, 260, 520, 1040 and 5200 pNm s, respectively. The grey area indicates the 90° frontal window used to score fixation behaviour.

Fig. 7A). None of the 24 tested flies showed fixation at the lowest damping coefficient (52×10^{-12} Nm s), whereas we obtained the maximum index of 76% at a damping coefficient of 1040×10^{-12} Nm s (blue, Fig. 7A). By contrast, anti-fixation behaviour steadily increased with increasing damping, suggesting that at least part of the decrease in fixation behaviour at dampings between 1024 and 5200×10^{-12} Nm s is due to an increasing preference of the fly to steer away from the visual target (linear regression fit, $y=-0.03+1.36\times10^{3}\log(x)$, $R^2=0.96$, $P<0.0001$; red, Fig. 7A).

The decrease in fixation index with decreasing damping below 1040×10^{-12} Nm s corresponds to an increase in azimuth velocity of the visual panorama (Fig. 7B), superficially suggesting that the decrease in visually mediated performance is due to the limits of visual motion detection (linear regression fit, $\log(y)=5.6-1.06\log(x)$, $R^2=0.96$, $P<0.0001$; red, Fig. 7B). Panorama velocity differed by approximately a factor of 100 between the highest and the lowest damping coefficients. By contrast, during fixation behaviour we found no significant difference in azimuth velocity among the damping coefficients (one-way ANOVA: $F_{6,36}=2.74$, $P=0.15$). Instead, the absolute angular velocity was relatively constant, yielding 210±48 deg. s^{-1} among the various coefficients ($N=7$ damping coefficients, blue, Fig. 7B). As expected from the previous figures, the mean position probability of the stripe in all tested flies co-varied with fixation index, as shown by the position histogram in Fig. 7C.

Since one goal of this study was to investigate the changes in wing kinematics with changing frictional damping, we plotted stroke frequency, the sum of stroke amplitude and the relative difference in amplitude of both wings, i.e. proportional to yaw torque (Fig. 8A–C). The data show that wing stroke frequency remains approximately constant during turning behaviour (200–215 Hz, Fig. 8A) because we found no statistical

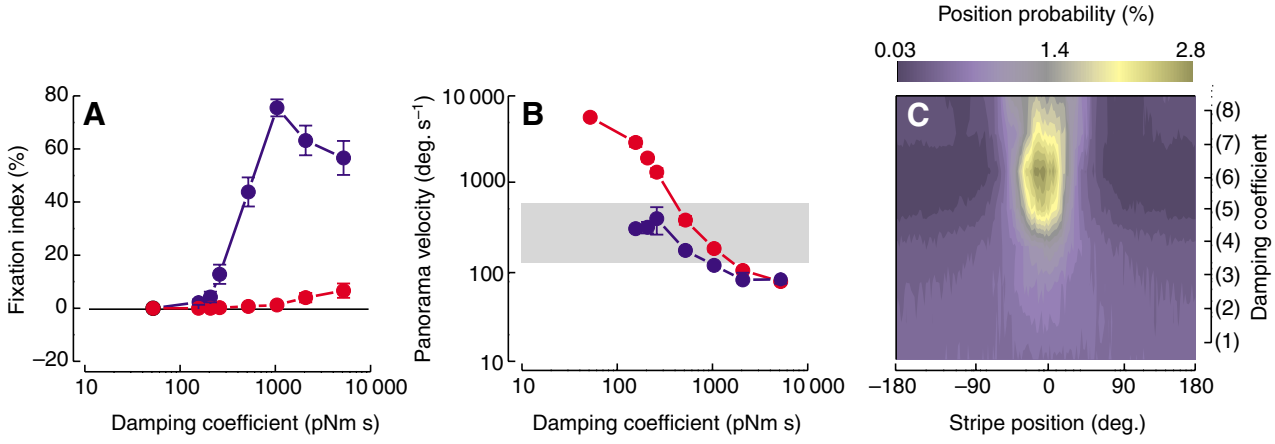

Fig. 7. Mean data of the tested flies responding to the black stripe displayed in the simulator at various frictional dampings. (A) Index of fixation (blue) and antifixation (red), calculated from the times the flies kept the stripe in the 90° frontal or caudal region of their the visual field, respectively. (B) Mean rotational velocity of the visual panorama during fixation (blue) and times without fixation behaviour (red). Grey area indicates threshold range of the visual system (cf. Materials and methods). (C) Relative probability of mean stripe position of the complete flight sequences plotted in pseudo-colour. Numbers in parentheses correspond to damping coefficients as listed in the legend to Fig. 3. Values are means ± s.e.m., $N=24$ flies.

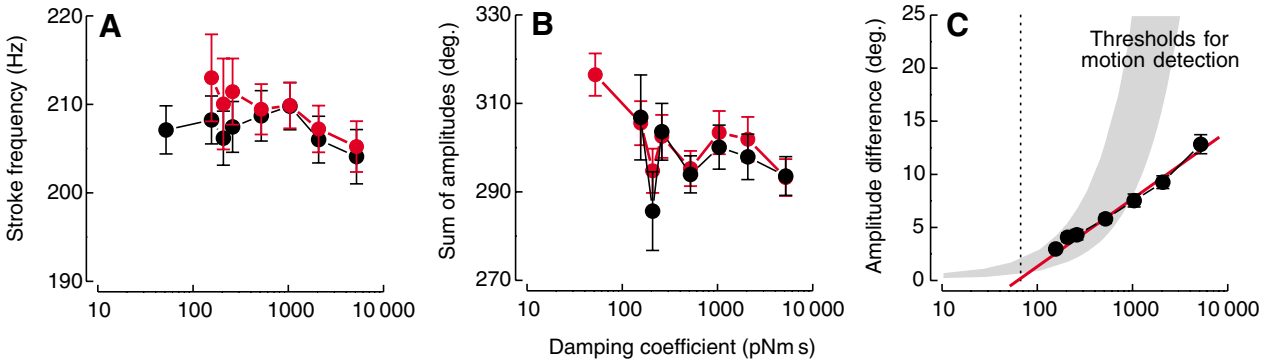

Fig. 8. Mean wing kinematics during object orientation behaviour plotted as a function of the simulated damping coefficient. (A) Stroke frequency, (B) sum of left and right stroke amplitude, (C) absolute difference between left and right wing stroke amplitude. Linear regressions fit to measured data is shown in red while the shaded area indicates the upper limits of the visual system that allows visual control of the stripe (Eqn 5; 50 and 100% threshold). Dotted line in C indicates where the regression line crosses with the *x*-axis. Values are means ± s.e.m., *N*=24 flies.

difference between (i) the frictional damping coefficients ($F_{6,36}$=1.03, P=0.43) and (ii) fixation behaviour (red) and data averaged over the entire flight sequence (black, $F_{1,6}$=1.06, P=0.34, Fig. 8A). This finding is consistent with other studies on flight behaviour, showing that stroke frequency is only modulated during the control of total flight force (Götz, 1968; Lehmann and Dickinson, 1998; Lehmann and Dickinson, 2001). Similar to frequency, the sum of left and right stroke amplitudes varied only slightly in the range between 300 and 320° in response to different damping coefficients (Fig. 8B), and did not significantly change with frictional damping except for the data at 208×10^{-12} Nm s ($F_{6,36}$=3.41, P=0.01).

By contrast, while fixating on the vertical stripe, the flies markedly decreased the difference in stroke amplitude between their two wings with decreasing damping coefficient (linear regression fit, $y=-10\times6.1\log(x)$, R^2=0.98, P<0.0001; Fig. 8C). This was expected because elevated friction requires higher yaw torque in order to move the stripe inside the simulator. On the logarithmic scale, the linear regression line intercepts the *x*-axis at 52×10^{-12} Nm s. This suggests that at small frictional damping coefficients, fruit flies must reduce their relative wing stroke amplitude to relatively small values in order to keep the angular rotation of the stripe below the threshold of the visual system. We plotted the visual threshold as a grey area in Fig. 8C for the two estimates of visual motion detection (50 and 100% EMD response). According to Eqn 5, the theoretical maximum for relative stroke amplitude for visually mediated yaw–torque steering is 8° and 25° at the best fixation index (1040×10^{-12} Nm s) for 100% and 50% response threshold (Fig. 7A), respectively, which nearly matches the mean relative stroke amplitude of 7.4±3.0° (*N*=25 flies) found in *Drosophila*. Since some flies maintained fixation behaviour down to 156×10^{-12} Nm s, it seems that they are able, at least for a short time, to control relative stroke amplitude on average within a range of 2.9±0.8° (*N*=8 flies) and thus within the theoretical range of 1–4° amplitude. If we extrapolate the visual thresholds in Fig. 8C to smaller values using Eqn 5, however, we find that for the natural damping coefficient of *Drosophila* as estimated in this

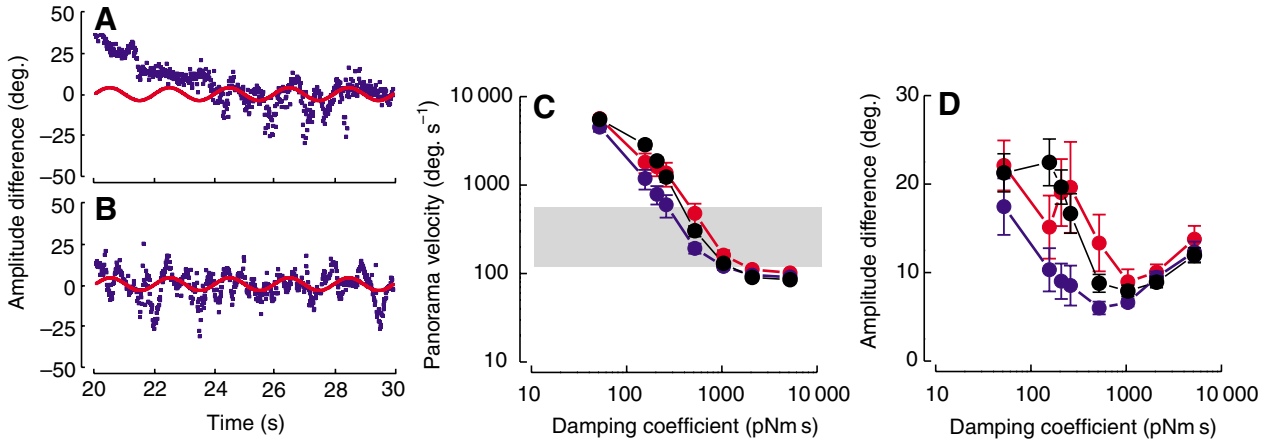

Fig. 9. Response of *Drosophila* (blue) to a velocity bias on two random-dot backgrounds at different dampings. Amplitude response (left-minus-right) to a low- (A; pattern shown in Fig. 1C) and high-contrast panorama (B; pattern shown in Fig. 1D). (C) Mean values of panorama velocity and (D) mean relative amplitude difference, both plotted as a function of frictional damping coefficient. Data are mean values of entire flight sequences using low- (red) and high (blue) contrast pattern and during object orientation behaviour (black). Grey area indicates threshold range of the visual system (cf. Materials and methods). For more details, see legend to Fig. 4. Values are means ± s.e.m., *N*=24 (black), *N*=8 (red), and *N*=15 flies (blue).

study (54×10^{-12} Nm s), the maximum difference in stroke amplitude should be in the range of 0.5–1.7° or approximately 0.25–0.85° amplitude for each wing. Assuming the frictional damping coefficient for the body alone (0.52×10^{-12} Nm s), our model even requires the control of relative stroke amplitude with a minimum precision of 0.1– 0.4°.

Optomotor experiments

As a possible reason for the breakdown in visually mediated object orientation response at low damping coefficients, we considered the difficulty of the fly to stabilize the random-dot background pattern while fixating the black stripe. To compare the performance of flies responding to small-field visual input with animals using large-field input, we tested fruit flies on their ability to compensate for the azimuth velocity bias on two random-dot patterned backgrounds (Fig. 9A,B). Fig. 9C shows that angular velocity of the visual panorama averaged over the entire flight sequences significantly decreases with increasing damping coefficient during both fixation and optomotor behaviours ($F_{7,308}$=153.7, P<0.001, linear regression fit: y=6.1–10log(x), R^2=0.98, P<0.0001, N=7). In general, the differences in angular velocity between object orientation and optomotor experiments were relatively small, but our statistical analysis revealed two major statistical effects: (i) angular velocity of the high-contrast pattern (black) was smaller than the velocity of low-contrast backgrounds used for object orientation (black) and optomotor (red) stimulation ($F_{2,44}$=8.16, P=0.001), and (ii) angular velocity of the virtual panorama during fixation experiments did not differ from those found in experiments using the same background, but without the foreground stripe (Tamhane *post hoc* test).

The findings on wing kinematics during optomotor stimulation were rather similar to those derived from object orientation experiments and may be summarized as follows. (i) Wing stroke frequency for all experiments and damping coefficients ranged between 195 and 215 Hz but neither the frequencies obtained at the various dampings ($F_{2,44}$=1.40, P=0.26) nor the frequencies at the three experimental conditions ($F_{14,308}$=1.53, P=0.14) were significantly different. (ii) The sums of left and right stroke amplitude during optomotor response were in the range of 280° and 320° amplitude and not statistically different between the damping coefficients ($F_{14,308}$=1.73, P=0.10) or between the three experimental conditions ($F_{2,44}$=1.08, P=0.35). (iii) Under all three experimental conditions, the relative difference in wing stroke amplitude significantly depended on frictional damping ($F_{7,308}$=16.59, P<0.001), and the Tamhane *post hoc* test showed that the amplitude response due to the high-contrast visual pattern was significantly different from the flight data obtained with the low-contrast background patterns (Fig. 9D). On average, at low frictional damping coefficients between 52 and 520×10^{-12} Nm s the difference in relative amplitude between the two optomotor patterns amounted to approximately 7.6±2.9° (N=5 dampings).

Quantification of visually mediated behaviour

The major goal of this study was to evaluate the behavioural responses of fruit flies to changes in damping coefficient for yaw during turning behaviour. To quantify the ability of the animals to control the angular velocity and acceleration of the visual panorama at the various coefficients, we developed a numerical model that predicts the relative difference in wing stroke amplitude required to fully compensate the azimuth velocity bias to the visual panorama (Eqn 9 in the Materials and methods). The performance of the fly may then be derived from the differences in relative amplitude between both wings and the model predictions at both fixation and optomotor behaviours. These data are shown in Fig. 10, plotted as a function of the simulated frictional damping. The U-shaped curves suggest that under all experimental conditions, the deviations of stroke amplitudes from the model predictions are lowest at frictional damping between 520 and 1040×10^{-12} Nm s, which is approximately 10–20 times the value of the expected natural damping coefficient. We found that the differences were significantly different among various damping coefficients ($F_{7,308}$=30.78, P<0.001) and also between the three experimental conditions ($F_{2,44}$=5.86, P=0.006). We measured best flight performance in the high-contrast random-dot environment, which yielded a minimum mean deviance in stroke amplitude of approximately 5° at 520×10^{-12} Nm s. In general, mean deviances between experiment and model prediction averaged over all damping coefficients were 16.4±6.7°, 17.6±6.5° and 11.7±6.6° for object orientation, low- and high-contrast optomotor stimulation, respectively.

Discussion

In the present study we investigated the significance of frictional damping for yaw turning behaviour in the fruit fly *Drosophila*. To quantify the behavioural effects we scored the tethered animals on their ability to stabilize both a visual target in the frontal position and two different random-dot patterns displayed in a flight simulator. To continuously face the animals with a steering task, we applied a sinusoidal azimuth velocity bias to the patterns. In both experimental approaches we found that the flies minimize the bias best at a damping coefficient between 520 and 1040×10^{-12} Nm s, which is at least one decade above a value estimated for friction on the *Drosophila* body including its wings. Moreover, the kinematic analyses in Fig. 8, in conjunction with the modelling of visual motion detection, suggest that flight control at natural damping might be constrained by the precision of stroke amplitude control rather than by the limits of the visual system *per se*. In the following sections we discuss these findings in greater detail and also the impact of our new estimate of frictional damping for the need to actively brake during a saccade.

Visual threshold and precision of motor control

A common feature of all experimental results was the ability of the flies to minimize the velocity bias over a large range of damping coefficients. However, visually mediated control broke down at low coefficients close to the natural value and at unnaturally high damping coefficients, presumably for two distinct reasons. At the high end of damping, the animals failed to compensate for the velocity bias because they had reached their maximum locomotor capacity for steering. Fig. 4F implies that this limit is approximately at ±25° relative difference in stroke amplitude, which is similar to the results of previous studies (Lehmann and Dickinson, 2001; Götz, 1983). By contrast, at the low end of frictional damping, object orientation

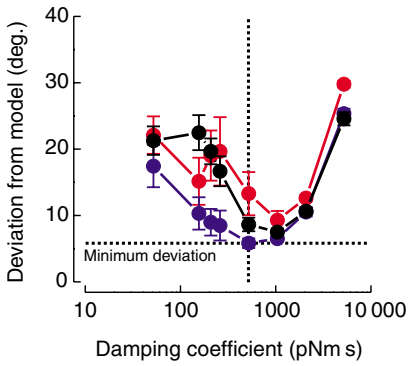

Fig. 10. Deviation of measured, absolute stroke amplitude between both wings from the numerical model, which predicts the wing motion required to compensate for the velocity bias. Object orientation and optomotor experiments using low (high) contrast patterns are plotted in black and red (blue), respectively. Mean minimum deviation at 520 pNm s damping coefficient amounted to approximately 6°, while the animals responded to the bias applied to the high-contrast background (blue). Values are means ± s.e.m., N=24 (black), N=8 (red) and N=15 flies (blue).

behaviour and stabilisation performance might be constrained either by the difficulty of the visual system to encode high angular velocities and/or by the muscle system to modulate wing stroke amplitudes with the required precision. In other words, our modelling (Eqn 5, Fig. 8C) implies that visually mediated turning control results from both the properties of the visual system to detect visual motion with a short response time and the ability of the fly's steering muscles to minimize the amplitude changes required for torque control. Interestingly, Figs 4–7 show that the fly managed to keep the angular velocity of the panorama relatively constant across all damping coefficients during object fixation and below a visual threshold of approximately ±250–300 deg. s^{-1}. Thus, even at damping values close to the natural estimate, the simulator data suggest that the animal apparently still uses visual feedback for turning control when orientating towards the visual target.

If we assume that the fruit flies are not limited by the visual system *per se* under our experimental conditions, we may alternatively hypothesise that turning performance is limited by the ability of the animal to control the difference in stroke amplitude below approximately 3°, or 1.5° in each wing (Fig. 8C). This value corresponds to approximately 6% of the fly's kinematic envelope for yaw steering (25°, Fig. 4). Since we did not find animals that were able to keep the stripe in the frontal window using mean relative differences below this value, the suggested value might represent the absolute lower threshold for amplitude control in *Drosophila*. For comparison, our model (Eqn 5) predicts a maximum amplitude difference at the natural damping coefficient of 54×10^{-12} Nm s between approximately 1 and 2°. Previous studies on stroke amplitude modulation in response to visual stimuli in fruit flies often scored amplitudes in relative units or voltage (Heide and Götz, 1996; Sherman and Dickinson, 2003; Sherman and Dickinson, 2004; Tammero and Dickinson, 2002a) and only very few authors calibrated these readings into changes in degrees. For example, Götz and co-workers (Götz et al., 1979) found 6–12° differences in wing stroke amplitude in tethered fruit flies during optomotor behaviour, and Fry and coworkers (Fry et al., 2003) found a rather similar maximum value during a free flight saccade of 6–10°, despite the different measurement techniques and flight conditions used. Thus, a mean value of 3° is below mean values typically reported for fruit flies during yaw turning.

If we conclude that fruit flies cannot achieve visually mediated flight control at their natural damping coefficient in the simulator, however, the question arises how these animals stabilize their yaw direction in free flight. The most obvious explanation would be that in the simulator, the flies can only steer by changing their stroke amplitudes. Since multiple studies have shown that insects use a large variety of kinematic mechanisms, we cannot exclude that fine control of yaw torque is mediated by other parameters than amplitude, such as rotational speed and timing at the stroke reversals (cf. Introduction). Pilot experiments in our simulator, however, show that dorsal flip timing is tightly correlated with stroke amplitude and presumably may not be used independently for flight control (linear regressions fit, mean R^2=0.47, mean P<0.001, N=6 coefficients) (Balint and Dickinson, 2001; Balint and Dickinson, 2004; Dickinson et al., 1993). In the following section we discuss three remaining possible explanations for the outcome of our study: (i) the role of the visual structure of the panorama, (ii) potential errors involved in the estimation of the natural damping coefficient, and (iii) the role of the halteres for flight stabilization.

The role of the visual panorama

Previous behavioural studies emphasized that saccadic flight in freely flying fruit flies and optomotor response in tethered flies depend on the structure of the visual environment and the size of the stimulated eye region (Tammero and Dickinson, 2002b; Heisenberg and Wolf, 1984). We thus considered the limited visual feedback provided by the single stripe as a possible reason for the failure of the flies to compensate for the azimuth bias in the object orientation experiments at low frictional damping. Since the stripe only stimulated a limited number of elementary motion detectors, the expected low signal-to-noise ratio in the visual neuropil might have hindered the animal from extracting the motion stimulus from the background noise with short temporal delay (Haag et al., 2004).

An alternative explanation would be that the fly performed suboptimally in response to the relative motion between the foreground object (stripe) and background (low-contrast random dots). Evidence for both views were derived from our optomotor experiments, showing that the fly's relative wing stroke amplitude differences are significantly lower during flight in response to the high-contrast 360° panorama than during object orientation behaviour (Fig. 9). Direct comparisons of mean performance derived from the entire flight sequences suggest that improving the visual contrast of the background panorama without facing the fly with the task to visually keep the stripe in the frontal position resulted in a better stabilisation of the pattern (Fig. 10). We thus hypothesize that the relative contribution of the vision system to flight control in a freely flying animal increases with an increase in structural richness and contrast of the visual panorama, enhancing both the signal-to-noise ratio of motion detection and the visuo-motor response time to the motion stimuli. This hypothesis is similar to what was predicted for the visually mediated activation of the landing

response in house flies due to frontally expanding visual flow fields (Borst, 1990).

Estimation of frictional damping coefficient

Another explanation for the discrepancy between the simulator experiments and the performance required for free flight is that we may have underestimated the value of the natural damping coefficient. In Fig. 2 we demonstrated the effect of alterations in the eight major parameters used for the numerical model. Although none of these changes could alter the damping coefficient more than fivefold in the range of parameters reported for the fruit fly, centre of pressure and the ratio between up- and downstroke may have a strong influence on the model prediction. Although there is no indication yet that these parameters vary tremendously during free flight, Ramamurti and Sandberg reported changes in pressure distribution on the wings within the saccade, employing an elaborate 6-DoF computational fluids model (Ramamurti and Sandberg, 2007). The authors showed that within the saccade manoeuvre, the pressure distribution on the left and right wing did not show any symmetry during the cycle, with the bottom left wing showing higher pressure extending over a larger region. In comparison, pressure distribution on the surface of wings in a hover cycle without yaw turning is almost symmetrical between both wings. During hovering, the location of the centre of pressure (CP) thus nearly coincided between left and right wing, whereas during yaw turning CP varied throughout the 90° saccadic turn. These variations, however, were relatively minor and amounted to peak-to-peak fluctuations of only 0.25 mm or 1/10 wing length (cf. Fig. 3D). Some extreme cases in up- and downstroke ratios have been reported in tethered flying fruit flies [f=0.54–0.80 (Zanker, 1990)].

Besides the above considerations, our numerical model simplified some aspects that might have resulted in an underestimation of damping coefficient. (i) We used quasi-steady aerodynamics on averaged values of wing speed and torque throughout the wing stroke, thus ignoring the temporal substructure of wing and body dynamics. (ii) We ignored inertial effects of the fly body, assuming a constant angular velocity during a saccade following the findings of Fry et al. (Fry et al., 2003), although other studies suggest continuous changes in angular velocity within a saccade, as already mentioned in the Materials and methods (M. Mronz and F.-O. Lehmann, manuscript submitted for publication) (Tammero and Dickinson, 2002b). (iii) In our model we used a mean profile drag coefficient of approximately 1.5, derived from a model wing flapping with an average *Drosophila* kinematic pattern (Dickinson, 1999; Fry et al., 2005) (Table 1). However, the mean drag coefficient depends on ventral and dorsal flip start and timing, and other studies reported a profile drag coefficient of approximately 3.0 for a similar kinematic pattern, which doubles our estimate for natural damping in *Drosophila* (Fig. 2D) (Sane and Dickinson, 2001). Altogether, given the above uncertainties in the estimation of the damping coefficient, we cannot fully exclude that *Drosophila* is capable of visually controlling its environment in our experiments at its natural damping coefficient even without using gyroscopic halters for feedback control. However, since our estimate is close to a previous study on a tethered, but freely rotating fly, it seems unlikely that we underestimated the natural damping coefficient by a factor of 5–10 (Mayer et al., 1988). This factor would be necessary for visual control of prolonged flight sequences of tethered *Drosophila*.

The role of the halteres

The main difference between tethered and free flight experiments is the lack of mechanosensory feedback from the halteres in the tethered animal (Pringle, 1948). Flies with ablated halteres show only very short and chaotic flight sequences in free flight and longer, but disturbed flights in tethered flight (T.H., unpublished observations) (Bender and Dickinson, 2006b; Dickinson, 1999; Dickinson, 2005). Histological reconstructions highlighted a direct neural pathway from the halteres to the motor neurons of the basalare 1 steering muscle (Fayyazuddin and Dickinson, 1996) that plays an important role in modulating the wing kinematics (Tu and Dickinson, 1996; Balint and Dickinson, 2004).

Potentially, there are two major mechanisms by which the haltere might improve the fine control of wing stroke amplitude. (i) The sensory output of the halteres connects to the steering muscle motoneurons *via* electrical synapses, which potentially increases the accuracy with which rotational velocity is transmitted to the steering muscles, although there is no present evidence for this view (Fayyazuddin and Dickinson, 1996). (ii) The haltere system encodes for much higher angular velocities and also responds faster than the visual system (Bender and Dickinson, 2006a; Sherman and Dickinson, 2003; Sherman and Dickinson, 2004). For example, Hengstenberg et al. (Hengstenberg et al., 1986) found that mechanical stimulation of the halteres induces head movements within 5 ms or approximately 6 times faster than the visuo-motor response time *via* the compound eyes (Land and Collett, 1974). Eqn 5 suggests that a response time within the range of a single wing stroke (5 ms) would allow larger differences in stroke amplitude for yaw control. Consequently, a fruit fly exhibiting a 5 ms response time of the visual system might keep angular velocity of the panorama below the threshold of the visual system even at its natural damping coefficient, because the required relative difference in stroke amplitude for fixation behaviour would be close to the range between 1.2° and 3.7° and thus in the range of visually mediated yaw control (Fig. 8C).

The consequences of the damping coefficient for yaw control

In this section we discuss the impact of our high frictional damping coefficient on saccadic turning behaviour in *Drosophila* and thus on the question of whether flight in fruit flies is dominated by the moments of inertia or frictional damping. The latter controversy was recently fuelled by Fry et al. (Fry et al., 2003), who estimated a frictional damping coefficient for *Drosophila* of 0.52×10^{-12} Nm s. The most prominent implication of that finding was that fruit flies should actively terminate saccadic rotation (counter-torque) due to low air friction. According to our data, angular acceleration of the panorama is 5–20 times larger than the angular velocity for all damping coefficients. Since we found that the damping coefficient of the body including the wings (54×10^{-12} Nm s) is more than 100 times larger than inertia, the damping term in torque (Eqn 1) is roughly 4–16 times larger than the inertia term. This suggests that

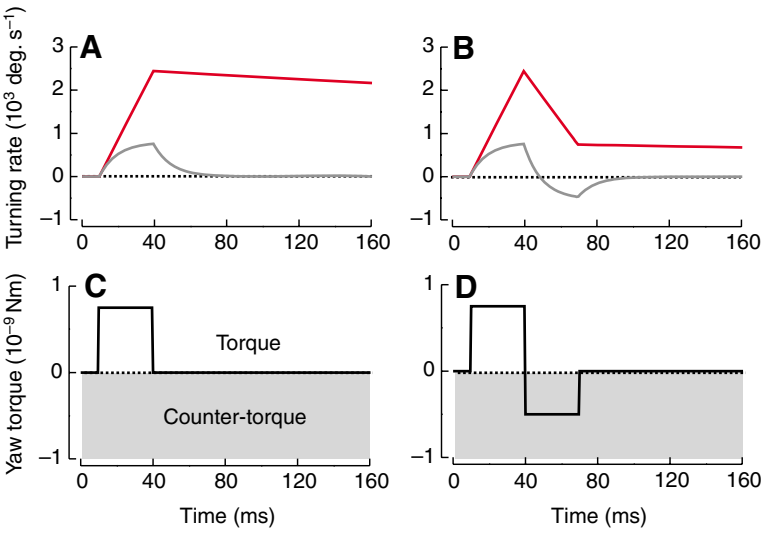

Fig. 11. Numerical modelling of a flight saccadic in *Drosophila*. (A–D) Time courses of turning rate in response to torque without counter-torque (A,C) and with counter-torque (B,D). Data are plotted at low (red line, 0.52 pNm s) and high (grey line, 54 pNm s) damping coefficient. The torque profile in D was averaged from Fig. 3C in Fry et al. (Fry et al., 2003), reported for a freely flying fruit fly. Turning rate was calculated from Eqn 4 and moment of inertia was 0.52 pNm s^2.

friction plays a larger role in determining flight forces during turning in *Drosophila* than inertia, which runs counter to the previous assumption, or in other words: using a damping coefficient of 54×10^{-12} Nm s and Fry's data on torque would result in a saccadic turn of approximately 18°. During a saccade, however, the fly turns approximately 90° within 50–100 ms, reaching a maximum turning rate of approximately 1600° s^{-1} (Fry et al., 2003; Tammero and Dickinson, 2002b). Since a detailed reconstruction of the manoeuvre in free flight showed that it takes approximately 15 ms at the end of the saccade before the fly completely stops turning, the authors argued that, given the low damping coefficient, friction is not sufficient to passively stop rotation (Fry et al., 2003). Thus, fruit flies produce a counter-torque to decelerate, presumably mediated by haltere feedback (Dickinson, 2005). This hypothesis would explain why saccades in tethered flight, without haltere feedback, take almost 10 times longer than in free flight (Heisenberg and Wolf, 1979; Tammero and Dickinson, 2002a). Although a study on saccade dynamics employing a magnetic tether apparently confirmed the idea of active braking, the torque estimates in this study were 10-times smaller than the values estimated for the freely flying animal (Bender and Dickinson, 2006a).

To resolve these discrepancies, we modelled the angular velocity profile during saccadic rotation using Eqn 4 and yaw torque profiles without (Fig. 11A,C) and with counter-torque (Fig. 11B,D). The counter-torque profile had similar characteristics to what was estimated by Fry et al. for a dynamically scaled *Drosophila* model wing (Fry et al., 2003). The modelling shows that damping on the body alone (red line) does indeed require active braking to finish a saccade within the measured time frame. Without this active component, it would take approximately 2.3 s to reduce angular velocity to 10% of its maximum value. A damping coefficient based on the body and the flapping wings, however, passively brakes by friction alone and reduces angular velocity to 10% in only 23 ms, independent of peak angular velocity during rotation. Surprisingly, this value is close to the 15 ms reported by Fry et al. and suggests that active braking is probably not a necessary manoeuvre for a fruit fly to terminate yaw turning motion.

Another unresolved issue regarding saccade dynamics is the shape of the angular velocity profile. Two different profiles for

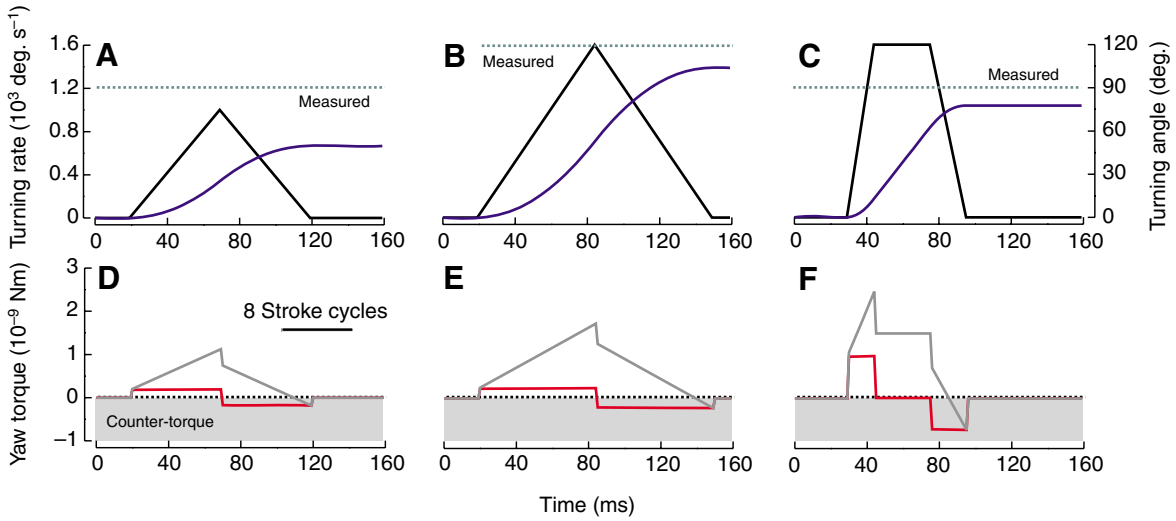

Fig. 12. Numerical modelling of free flight saccades in *Drosophila*. (A–C) Profiles of turning rate (black line, left scale) found in three previous studies; (A) (Tammero and Dickinson, 2002b), (B) M. Mronz and F.-O. Lehmann (manuscript submitted for publication) and (C) (Fry et al., 2003). Turning angle (blue line, right scale) was calculated from turning velocity. Broken green line indicates reported turning angle. (D–F) The corresponding torque profiles were derived from Eqn 1 at 0.52 (red line) and 54 pNm s damping coefficient (grey line). Note the mismatch in the measured final turning angle and the angle calculated from the velocity profile in A.

freely turning fruit flies have been reported: (i) Tammero and Dickinson estimated a triangular velocity profile with a maximum turning rate of 1000 deg. s^{-1} and duration of 100 ms (Fig. 12A) (Tammero and Dickinson, 2002b); M. Mronz and F.-O. Lehmann (manuscript submitted for publication) measured the same profile with a peak velocity of 1600 deg. s^{-1} and 130 ms duration (Fig. 12B); a triangular velocity profile was also measured in magnetically tethered flies (Bender and Dickinson, 2006a; Bender and Dickinson, 2006b). (ii) By contrast, Fry et al. found that turning rate is approximately constant within the saccade with sharp transients at the beginning and the end (Fry et al., 2003). According to these data angular velocity increases within 15 ms, exhibiting a constant velocity of 1600 deg. s^{-1} for 30 ms and finally decreases back to 0 deg. s^{-1} within 20 ms (Fig. 12C).

By integrating over the velocity profiles we may obtain the total angle of body rotation (Eqn 2 and Eqn 4; blue, Fig. 12A–C). The simulation shows that there is a fairly good match between the measured (green) and derived (blue) values for body rotation (Fig. 12B, 120° *vs* 104°; Fig. 12C, 90° *vs* 78°; measured *vs* simulated value) except for the first profile (Fig. 12A, 90° *vs* 50°). We thus assume that the first study underestimated peak angular velocity due to data acquisition (low sampling frequency) or data processing (low pass filtering). From the velocity and position data, we eventually calculated the underlying torque profiles at the two damping coefficients: 0.52 (body alone) and 54×10^{-12} Nm s (body and wings, Eqn 1). In all cases, a low frictional damping coefficient required peak torques between approximately 0.2 and 1.0×10^{-9} Nm, which corresponds to a relative difference in stroke amplitude of 0.7–3.4° (Eqn 2). By contrast, the high damping coefficient relies on peak torques between 1.0 and 2.2×10^{-9} Nm, corresponding to an amplitude differences of only 3.4–7.6°, close to the relative amplitudes described for free flight (Fry et al., 2003). Moreover, the torque profile measured by Fry et al. is more similar to the high damping than to the low damping torque profiles and mean torque for the high damping is also more in the range of the maximum torque measured in tethered *Drosophila* [±2.0–3.0×10^{-9} Nm (Heisenberg and Wolf, 1984)].

In addition, a more recent and elaborate three-dimensional computational fluid dynamic (CFD) study on *Drosophila* yaw turning (Ramamurti and Sandberg, 2007) supports our elevated damping coefficient for the fruit fly. The yaw torque estimated in this study requires a much higher damping coefficient than the value proposed by Fry et al., of approximately 29×10^{-12} Nm s to turn the animal 100°. Consequently, the torque profile shown in fig. 9C of the study by Ramamurti and Sandberg is more similar to that shown in Fig. 11A of the present study (no active braking), than to the biphasic profile measured in the robotic wing (Fry et al., 2003). Nevertheless, peak torque derived from the CFD study amounts to approximately 2.0×10^{-9} Nm and is consistent with the predicted estimation for peak torque during the saccadic turn in Fig. 12E [1.8×10^{-9} Nm; kinematics from M. Mronz and F.-O. Lehmann (manuscript submitted for publication)], work by Heisenberg and Wolf (Heisenberg and Wolf, 1984) and even the peak value measured by Fry and colleagues (data not shown). In general, the variety of saccadic profiles found in fruit flies appears to be surprising and emphasizes the needs for more kinematic data on freely manoeuvring animals in which the variations in both torque and rotational velocity profiles are measured with high precision.

Conclusions

This study on the significance of damping coefficient in a flying insect has provided several new insights into how turning behaviour of small animals depends on both the size and the kinematic pattern of their flapping wings. Our experiments suggest that tethered *Drosophila* fail to visually control yaw turning at its natural frictional damping coefficient whereby flight control may be restored by slightly increasing this measure. According to our numerical model, the wings in *Drosophila* contribute around 100 times more to total damping coefficient than the body alone. Consequently, the insect might dynamically change its damping coefficient, at least to some degree, by adjusting certain aspects in wing motion, such as up- to downstroke ratio. On the one hand, a high damping coefficient is beneficial because it may reduce the need for fast-reacting sensor systems like gyroscopic halteres and also reduces muscular precision needed for yaw control. On the other hand, elevated damping also lowers manoeuvrability by limiting the maximum rotational velocity that an insect may achieve, leaving the animal more vulnerable in air combats or during prey catching.

Flies that rely on high angular acceleration and turning rates need to have a precise flight apparatus by allowing either a higher spatial resolution in wing amplitude control and other kinematic parameters, or a higher temporal resolution by decreasing the time lack in response time during sensory feedback using halteres. We thus hypothesize that insects without halteres achieve yaw stability mainly due to high frictional damping on their wings and body. Alternatively, even insects with four wings may possess mechanosensory devices similar to the halteres of flies. A recent study, for example, found that the antennae of hawk moths vibrate and probably experience Coriolis forces during aerial manoeuvres and thus work as gyroscopic sensors (Sane et al., 2007). In conclusion, our study emphasizes the need for a comparative approach on flight control that links an insect's manoeuvrability with (i) the physical properties of its body, (ii) the properties of the sensory organs and (iii) the precision with which the muscular system may control the movements of the wings. Eventually, such information will be useful not only for a better understanding of the evolution and mechanics of insect flight, but also for engineers who design biomimetic micro-air vehicles.

Appendix

Details of the damping coefficient model

According to Ellington (Ellington, 1984a), the mean velocity of a wing segment, $\bar{u}(r)$, at distance r from the wing base and exhibiting a sinusoidal velocity profile during up- and downstroke, may be written as:

$$\bar{u}(r) = \frac{1}{2}\left|\overline{\frac{\mathrm{d}\hat{\Phi}}{\mathrm{d}\hat{t}}}\right| \Phi n r , \qquad \text{(A1)}$$

where $|\overline{\mathrm{d}\hat{\Phi}/\mathrm{d}\hat{t}}|$ is dimensionless wing velocity and n is stroke frequency (Lehmann and Dickinson, 1998). During turning, the

wing stroke amplitudes in the global coordinate system passively change as a result of body rotation, Φ_P, and actively as a result of the difference in wing beat amplitude of the two wings, Φ_A (Fig. 3A). Following again Ellington's nomenclature (Ellington, 1984a), we expressed the effective frequency for the up- and downstrokes by $n/(1–\hat{t})$ and $n/\hat{t}$, respectively, where $\hat{t}$ is the relative time of the downstroke in a complete stroke cycle (0–1), and calculated wing velocity for a wing segment at the centre of air pressure, $\hat{r}_{CP}$, of the wing with length R. According to Eqn A1, wing velocity of the left wing during up-, $\bar{u}_{L,U}$, and downstroke, $\bar{u}_{L,D}$, thus yields:

$$\bar{u}_{L,U} = \frac{1}{2}\left|\overline{\frac{d\hat{\phi}}{d\hat{t}}}\right| (\Phi–\Phi_{P,U}+\Phi_A)\,\frac{n}{1-\hat{t}}\,\hat{r}_{CP}R \qquad (A2)$$

and

$$\bar{u}_{L,D} = \frac{1}{2}\left|\overline{\frac{d\hat{\phi}}{d\hat{t}}}\right| (\Phi+\Phi_{P,D}+\Phi_A)\,\frac{n}{\hat{t}}\,\hat{r}_{CP}R\,, \qquad (A3)$$

respectively. We obtained a similar set of equations for mean velocity of the right wing during up-, $\bar{u}_{R,U}$, and downstroke, $\bar{u}_{R,D}$, that was written as:

$$\bar{u}_{R,U} = \frac{1}{2}\left|\overline{\frac{d\hat{\phi}}{d\hat{t}}}\right| (\Phi+\Phi_{P,D}–\Phi_A)\,\frac{n}{1-\hat{t}}\,\hat{r}_{CP}R \qquad (A4)$$

and

$$\bar{u}_{R,D} = \frac{1}{2}\left|\overline{\frac{d\hat{\phi}}{d\hat{t}}}\right| (\Phi–\Phi_{P,D}–\Phi_A)\,\frac{n}{\hat{t}}\,\hat{r}_{CP}R\,, \qquad (A5)$$

respectively. We derived mean drag $\bar{D}$ acting on the flapping wings from a simple quasi-steady aerodynamic model based on wing velocity squared, which may be expressed by the following equation (Ellington, 1984b):

$$\bar{D} = \tfrac{1}{2}\rho\bar{C}_{D,Pro}\bar{u}^2S\,, \qquad (A6)$$

where ρ is the density of air, $\bar{C}_{D,Pro}$ is the mean profile drag coefficient of the wing and S is the area of a single wing. By combining Eqn A2–A6 and defining that drag is positive during the downstroke and negative during the upstroke, we obtained the difference in profile drag, $\bar{D}_{diff}$, between the two wings by the equation:

$$\bar{D}_{Dif} = \tfrac{1}{2}\rho\bar{C}_{D,Pro}S[\hat{t}\bar{u}^2_{L,D} + (1–\hat{t})\bar{u}^2_{R,U} – (1–\hat{t})\bar{u}^2_{L,U} – \hat{t}\bar{u}^2_{R,D}]\,. \qquad (A7)$$

To convert the bilateral difference in wing drag into yaw torque, we multiplied the drag differential with a moment arm approximately equal to the distance between the fly's centre of gravity (Lehmann and Pick, 2007) and the wing's centre of pressure. Since the length of the moment arm depends on stroke angle, we approximated the mean moment arm by 3.1 mm, assuming that thoracic width, W, and wing length are approximately 1.1 and 2.5 mm, respectively (Table 1). Since rotational velocity of the animal is constant for the majority of the saccade, the acceleration term in Eqn 1 amounts to zero and mean torque equals the product between frictional damping coefficient and mean rotational velocity. The combined frictional damping coefficient, C, for yaw turning of the fly body and the animal's wings thus is:

$$C = \frac{\bar{D}_{Dif}\hat{r}_{CP}(R+0.5W)}{\bar{\omega}} + C_B\,, \qquad (A8)$$

where C_B is the damping coefficient of the body alone, as derived from Stokes' law [0.52×10^{-12} Nm s (Fry at al., 2003)]. By inserting the values listed in Table 1 into Eqn A2–A5 and Eqn A8, we obtained a frictional damping coefficient of 54×10^{-12} Nm s. This value is more than 100 times the value estimated from the fly body but in good agreement with the results of an earlier study that reported an upper estimate of 57×10^{-12} Nm s for *Drosophila* (Mayer et al., 1988).

The authors thank Nicole Heymann for technical assistance, the students Natalia Merdian and Martin Schauflinger for their help with carrying out the experiments, and Ursula Seifert for critically reading the manuscript. This work was funded by the Biofuture grant 0311885 and Bionics grant 0313772 of the German Federal Ministry for Education and Research to F.O.L.

References

Alexander, D. E. (1986). Wind tunnel studies of turns by flying dragonflies. *J. Exp. Biol.* **122**, 81-98.

Autrum, H. (1958). Electrophysiological analysis of the visual system in insects. *Exp. Cell Res. Suppl.* **14**, 426-439.

Balint, C. N. and Dickinson, M. H. (2001). The correlation between wing kinematics and steering muscle activity in the blowfly *Calliphora vicina*. *J. Exp. Biol.* **204**, 4213-4226.

Balint, C. N. and Dickinson, M. H. (2004). Neuromuscular control of aerodynamic forces and moments in the blowfly, *Calliphora vivina*. *J. Exp. Biol.* **207**, 3813-3838.

Bender, J. A. and Dickinson, M. H. (2006a). A comparison of visual and haltere-mediated feedback in the control of body saccades in *Drosophila melanogaster*. *J. Exp. Biol.* **209**, 4597-4606.

Bender, J. A. and Dickinson, M. H. (2006b). Visual stimulation of saccades in magnetically tethered *Drosophila*. *J. Exp. Biol.* **209**, 3170-3182.

Berger, S. and Kutsch, W. (2003). Turning manoeuvres in free-flying locusts: high speed video-monitoring. *J. Exp. Zoolog. A Comp. Exp. Biol.* **299A**, 127-138.

Borst, A. (1990). Landen ohne Lotsen. *Biol. Unserer Zeit* **20**, 245-250.

David, C. T. (1978). The relationship between body angle and flight speed in free-flying *Drosophila*. *Physiol. Entomol.* **3**, 191-195.

Dickinson, M. H. (1999). Haltere-mediated equilibrium reflexes of the fruit fly, *Drosophila melanogaster*. *Philos. Trans. R. Soc. Lond. B Biol. Sci.* **354**, 903-916.

Dickinson, M. H. (2005). The initiation and control of rapid flight maneuvers in fruit flies. *Integr. Comp. Biol.* **45**, 274-281.

Dickinson, M. H., Lehmann, F.-O. and Götz, K. G. (1993). The active control of wing rotation by *Drosophila*. *J. Exp. Biol.* **182**, 173-189.

Dickinson, M. H., Lehmann, F.-O. and Sane, S. P. (1999). Wing rotation and the aerodynamic basis of insect flight. *Science* **284**, 1954-1960.

Dudley, R. and Ellington, C. P. (1990). Mechanics of forward flight in bumblebees. I. Kinematics and morphology. *J. Exp. Biol.* **148**, 19-52.

Ellington, C. P. (1984a). The aerodynamics of insect flight. III. Kinematics. *Philos. Trans. R. Soc. Lond. B Biol. Sci.* **305**, 41-78.

Ellington, C. P. (1984b). The aerodynamics of insect flight. IV. Aerodynamic mechanisms. *Philos. Trans. R. Soc. Lond. B Biol. Sci.* **305**, 79-113.

Ellington, C. P., Van den Berg, C., Willmott, A. P. and Thomas, A. L. R. (1996). Leading edge vortices in insect flight. *Nature* **384**, 626-630.

Fayyazuddin, A. and Dickinson, M. H. (1996). Haltere afferents provide direct, electrotonic input to a steering motor neuron in the blowfly, *Calliphora*. *J. Neurosci.* **16**, 5225-5232.

Fry, S. N., Sayaman, R. and Dickinson, M. H. (2003). The aerodynamics of free-flight maneuvers in *Drosophila*. *Science* **300**, 495-498.

Fry, S. N., Sayaman, R. and Dickinson, M. H. (2005). The aerodynamics of hovering flight in *Drosophila*. *J. Exp. Biol.* **208**, 2303-2318.

Götz, K. G. (1968). Flight control in *Drosophila* by visual perception of motion. *Kybernetik* **4**, 199-208.

Götz, K. G. (1983). Bewegungssehen und Flugsteuerung bei der Fliege *Drosophila*. In *BIONA Report 2* (ed. W. Nachtigall), pp. 21-34. Stuttgart: Fischer.

Götz, K. G., Hengstenberg, B. and Biesinger, R. (1979). Optomotor control of wing beat and body posture in *Drosophila*. *Biol. Cybern.* **35**, 101-112.

Haag, J., Denk, W. and Borst, A. (2004). Fly motion vision is based on Reichardt detectors regardless of the signal-to-noise ratio. *Proc. Natl. Acad. Sci. USA* **46**, 16333-16338.

Hardie, C. R. and Raghu, P. (2001). Visual transduction in *Drosophila*. *Nature* **413**, 186-193.

Hedrick, T. L. (2007). Experimental study of low speed turning flight in cockatoos and cockatiels. 45th AIAA Aerospace Sciences Meeting and Exhibit, 8-11 January 2007, Reno, Nevada, AIAA Paper 2007-44, www.aiaa.org.

Hedrick, T. L., Usherwood, J. R. and Biewener, A. A. (2007). Low speed maneuvering flight of the rose-breasted cockatoo (*Eolophus roseicapillus*). II. Inertial and aerodynamic reorientation. *J. Exp. Biol.* **210**, 1912-1924.

Heide, G. and Götz, K. G. (1996). Optomotor control of course and altitude in *Drosophila melanogaster* is correlated with distinct activities of at least three pairs of flight steering muscles. *J. Exp. Biol.* **199**, 1711-1726.

Heisenberg, M. and Wolf, R. (1979). On the fine structure of yaw torque in visual flight orientation of *Drosophila melanogaster*. *J. Comp. Physiol.* **130**, 113-130.

Heisenberg, M. and Wolf, R. (1984). *Vision in Drosophila*. Berlin: Springer-Verlag.

Hengstenberg, R., Sandeman, D. C. and Hengstenberg, B. (1986). Compensatory head roll in the blowfly *Calliphora* during flight. *Proc. R. Soc. Lond. B Biol. Sci.* **227**, 455-482.

Hollick, F. S. J. (1940). The flight of the dipterous fly *Muscina stabulens* Fallén. *Philos. Trans. R. Soc. Lond. B Biol. Sci.* **230**, 357-390.

Howard, J., Dubs, A. and Payne, R. (1984). The dynamics of phototransduction in insects: a comparative study. *J. Comp. Physiol. A* **154**, 707-718.

Kern, R. and Egelhaaf, M. (2000). Optomotor course control in flies with largely asymmetric visual input. *J. Comp. Physiol. A* **186**, 45-55.

Kutsch, W. and Gewecke, M. (1979). Development of flight behaviour in maturing adults of *Locusta migratoria*: II. Aerodynamic parameters. *J. Insect Physiol.* **25**, 299-304.

Land, M. F. and Collett, T. S. (1974). Chasing behaviour of houseflies (*Fannia canicularis*). *J. Comp. Physiol.* **89**, 331-357.

Lehmann, F.-O. and Dickinson, M. H. (1997). The changes in power requirements and muscle efficiency during elevated force productions in the fruit fly *Drosophila melanogaster*. *J. Exp. Biol.* **200**, 1133-1143.

Lehmann, F.-O. and Dickinson, M. H. (1998). The control of wing kinematics and flight forces in fruit flies (*Drosophila* spp.). *J. Exp. Biol.* **201**, 385-401.

Lehmann, F.-O. and Dickinson, M. H. (2001). The production of elevated flight force compromises manoeuvrabilitiy in the fruit fly *Drosophila melanogaster*. *J. Exp. Biol.* **204**, 627-635.

Lehmann, F.-O. and Pick, S. (2007). The aerodynamic benefit of wing-wing interactionsdepends on stroke trajectory in flapping insect wings. *J. Exp. Biol.* **210**, 1362-1377.

Marden, J. H. (1987). Maximum lift production during takeoff in flying animals. *J. Exp. Biol.* **130**, 235-258.

Mayer, M., Vogtmann, K., Bausenwein, B., Wolf, R. and Heisenberg, M. (1988). Flight control during 'free yaw turns' in *Drosophila melanogaster*. *J. Comp. Physiol. A* **163**, 389-399.

Pringle, J. W. S. (1948). The gyroscopic mechanism of the halteres of Diptera. *Philos. Trans. R. Soc. Lond. B Biol. Sci.* **233**, 347-384.

Ramamurti, R. and Sandberg, W. C. (2001). Computational study of 3-D flapping foil flows. 39th AIAA Aerospace Sciences Meeting and Exhibit, Reno, Nevada, Jan 8-11, 2001, AIAA-2001-605, www.aiaa.org.

Ramamurti, R. and Sandberg, W. C. (2007). A computational investigation of the three-dimensional unsteady aerodynamics of *Drosophila* hovering and maneuvering. *J. Exp. Biol.* **210**, 881-896.

Reichardt, W. and Poggio, T. (1976). Visual control of orientation behaviour in the fly. Part I. A quantative analysis. *Q. Rev. Biophys.* **9**, 311-375.

Sane, S. P. and Dickinson, M. H. (2001). The control of flight force by a flapping wing: lift and drag production. *J. Exp. Biol.* **204**, 2607-2626.

Sane, S. P., Dieudonne, A., Willis, M. A. and Daniel, T. L. (2007). Antennal mechanosensors mediate flight control in moths. *Science* **315**, 863-866.

Sherman, A. and Dickinson, M. H. (2003). A comparison of visual and haltere-mediated equilibrium reflexes in the fruit fly *Drosophila melanogaster*. *J. Exp. Biol.* **206**, 295-302.

Sherman, A. and Dickinson, M. (2004). Summation of visual and mechanosensory feedback in *Drosophila* flight control. *J. Exp. Biol.* **207**, 133-142.

Tammero, L. F. and Dickinson, M. H. (2002a). Collision-avoidance and landing responses are mediated by separate pathways in the fruit fly, *Drosophila melanogaster*. *J. Exp. Biol.* **205**, 2785-2798.

Tammero, L. F. and Dickinson, M. H. (2002b). The influence of visual landscape on the free flight behaviour of the fruit fly *Drosophila melanogaster*. *J. Exp. Biol.* **205**, 327-343.

Taylor, G. (2001). Mechanics and aerodynamics of insect flight. *Biol. Rev.* **76**, 449-471.

Tu, M. S. and Dickinson, M. H. (1996). The control of wing kinematics by two steering muscles of the blowfly (*Calliphora vicina*). *J. Comp. Physiol.* **178**, 813-830.

Vogel, S. (1994). *Life in Moving Fluids*. Princeton: Princeton University Press.

Wakeling, J. M. and Ellington, C. P. (1997). Dragonfly flight. II. Velocities, accelerations and kinematics of forward flight. *J. Exp. Biol.* **200**, 557-582.

Willmott, A. P., Ellington, C. P. and Thomas, A. L. R. (1997). Flow visualization and unsteady aerodynamics in the flight of the hawkmoth, *Manduca sexta*. *Philos. Trans. R. Soc. Lond. B Biol. Sci.* **352**, 303-316.

Zanker, J. M. (1988). How does lateral abdomen deflection contribute to flight control of *Drosophila melanogaster*? *J. Comp. Physiol. A* **162**, 581-588.

Zanker, J. M. (1990). The wing beat of *Drosophila melanogaster*. I. Kinematics. *Philos. Trans. R. Soc. Lond. B Biol. Sci.* **327**, 1-18.

Zarnack, W. (1988). The effect of forewing depressor activity on wing movement during locust flight. *Biol. Cybern.* **59**, 55-70.